Electronic Supplementary Material (ESI) for Journal of Analytical Atomic Spectrometry.

Supplementary Material

Instrument Design

Figure S-1 is a schematic diagram of our LA–ICP-DOFMS instrument. Details of the laser-ablation system are given in the experimental section of the primary report. Here, we briefly describe the design and operation of the ICP-DOF mass analyzer in order to familiarize readers with distance-of-flight mass separation. More detailed descriptions of the DOF mass-separation approach and the DOFMS instrument can be found in a number of publications.[1-6]

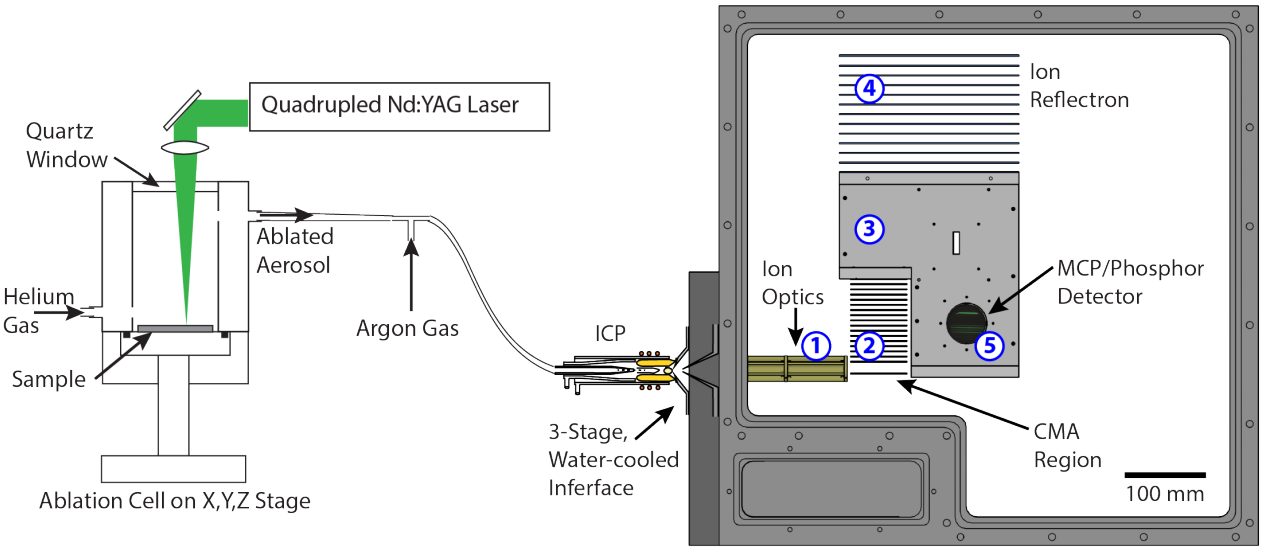

Figure S-1. Schematic diagram of the LA–ICP-DOFMS instrument. The laser-ablation setup and the ICP torch are not to scale. Instrument sections are numbered as referenced in the main text.

ICP–DOFMS Interface

The ICP was powered with a crystal-controlled RF generator (40.16 MHz, model HF 2000F, PlasmaTherm Inc, Kresson, NJ) with an automatic impedance matcher to minimize reflected power, and was created in a 1.5-mm central-channel-diameter quartz ICP torch (Precision Glass Blowing, Boulder, CO). A quartz torch bonnet and a copper torch shield were attached to the ICP torch to eliminate a secondary discharge at the sampler cone.[7-8] The plasma was sampled approximately 12 mm above the load coil by a 1-mm diameter nickel sampler cone; although the torch position was optimized daily to maximize signal. After the

sampler cone, ions were transferred into the mass analyzer through a differentially pumped skimmer-cone orifice followed by a third-stage, 1-mm diameter conductance-limiting aperture. The sampler and skimmer cones of the atmospheric-pressure interface were water-cooled to prevent melting. Pressures in the first, second, and third (mass analysis) stages of the instrument were maintained at 0.7, 4×10^{-4}, and 7×10^{-7} Torr, respectively.

DOF Mass Analyzer

One benefit of DOFMS is its simple instrument design: DOF mass separation is achieved as ions travel through, and are manipulated by, only five discrete instrument sections: 1. the input ion optics, 2. the constant-momentum acceleration (CMA) region, 3. the field-free (FF) flight region, 4. the linear-field ion mirror, and 5. the DOF extraction region and detector.

In the mass-analysis stage, ions are spatially focused into a tight ion beam into the CMA region with a dc quadrupole-doublet optics train. This spatial focus is critical because it limits the mass-separated ion-packet width on the DOFMS detector.[9] In the CMA region, ion packets are generated through periodically energizing the region; those ions within the CMA region at the onset of each CMA pulse are orthogonally accelerated into the field-free (FF) flight region with velocities inversely proportional to their *m/z* values. Constant-momentum acceleration is achieved by applying a linear electric field (E_p) across the acceleration region for a short enough time period (τ) such that all ions of interest are still *within* the acceleration region at the cessation of the pulse. The magnitude of momentum imparted is controlled by adjusting E_p and τ according to equation **1,** where q is the fundamental charge and z is the number of charges on the ion.

$$mv_{imp} = E_p \tau q z \qquad (\mathbf{1})$$

In the FF region, accelerated ion packets begin to separate according to their *m/z*-dependent velocities and then penetrate the linear-field ion mirror; this ion mirror has an electrostatic field-strength of E_M. Ions turn around in the mirror at energy-dependent depths and

are re-accelerated back into the FF region. In the second portion of the field-free region, after ions are reflected out of the mirror, all ions come into energy focus along the mass-separation axis at a single moment in time, called the energy-focus time (t_{ef}).[5] The t_{ef} is controlled by the amount of momentum imparted and the field-strength of the ion mirror according to equation **2**.

$$t_{ef} = \frac{4E_P\tau}{E_M} \qquad (\mathbf{2})$$

At the energy-focus time, all ions that have emerged from the ion mirror come into energy focus at *m/z*-dependent positions along the field-free region. By detecting the distance-of-flight of ions at t_{ef}, the adverse effects of the ions' initial kinetic energies on mass resolution are minimized and the distance ions have travelled (L_{FF}) is inversely proportional to *m/z*. Equation **3** is a simplified relationship between L_{FF} and *m/z*, where s_o is the distance ions travel in the CMA region.

$$L_{FF} = \frac{z}{m}\left(qE_p\tau\right)\left(\frac{2E_p\tau}{E_M} - \frac{\tau}{2}\right) - s_o \qquad (\mathbf{3})$$

In order to detect *m/z*-separated ion packets at t_{ef}, a second electrostatic acceleration region, called the DOF extraction region, is installed downstream of the ion mirror and is used to push a section of the *m/z*-separated ion beam onto a spatially selective detector so that ions land on the detector at t_{ef}. The DOFMS detector used here has been previously described[6] and consists of a pair of 40-mm microchannel plates (MCPs) arranged in a chevron configuration and a metallized phosphor screen stacked above the MCPs. The MCPs convert and amplify ion strikes into secondary electrons and the phosphor screen converts these secondary electrons into photons. Two microchannel plates are used here to get an ion-to-electron amplification factor of around $1\text{x}10^6$, and arranged in the chevron configuration to minimize ion feedback. Mass spectra are captured as images of the phosphor screen that are taken through a Plexiglas® viewport with a scientific CCD camera (iKon CCD, Andor Technologies plc., UK) positioned above the phosphor screen.

DOF Mass Spectrum Collection

In DOFMS, a "snapshot" of the total mass spectrum is recorded with the spatially selective detector. All ions recorded in this snapshot are obtained simultaneously; however, the range of *m/z* values detected in each DOFMS experiment is limited by the total flight distance of ions through the analyzer and the length of the DOF detector. In previous work, we found that the high-to-low mass range of our current DOFMS setup is 1.11; this is also confirmed by the work presented here.[6] While the high-to-low mass range is fixed on our DOFMS instrument, ions of any desired *m/z* value can be brought into focus on the DOFMS detector by adjustment of CMA and ion-mirror voltages to bring ions of interest into energy focus at an L_{FF} value that is within the bounds of the DOF detector. In this way, many regions of the DOF mass spectrum can be analyzed successively.[3]

In addition to mass-spectral coverage, the manner in which CCD images of the MCP/phosphor are captured partly determines detection characteristics such as temporal resolution, detection duty cycle, *S/N* ratio, and dynamic range. For both steady-state and single-pulse LA-ICP-DOFMS studies, the CCD exposure, acquisition speed, and acquisition timing were controlled in order to balance the *S/N* ratios and temporal resolution of the spectra. The iKon CCD camera has a native resolution of 1064x1064 pixels; however, for all studies reported here, the CCD was binned on-chip to either 512x512 or 256x256 pixels. While binning pixels sacrifices image resolution, it reduces camera read noise as well as the required readout time of the CCD, which, in turn, improves the DOF-detection duty cycle. For all DOFMS images here, a CCD-pixel readout rate of 3 MHz was used. In the steady-state LA studies, the CCD was binned to 512x512 pixels, which corresponds to a CCD readout time of 0.1674 s. In single-pulse LA, the CCD was binned to 256x256 pixels in order to reduce the CCD readout time to 0.09025 s. Combined with exposure times of 100-150 ms, DOFMS spectral acquisition speeds ranged from 5.25 to 4.16 Hz for single-pulse LA studies. This means that the CCD detector was

collecting images for 52% or 63% of laboratory time (the CCD was being read out the rest of the time). We call the percentage of exposed time by the CCD the DOF detection duty cycle, and it is an important consideration because it controls how efficiently DOFMS spectra are collected and thus impacts the analyzer's sensitivity.

Time-Delay Acquisition

As described in the primary report, the *S/N* ratio of LA–ICP-DOFMS spectra is improved when the spectra are collected with longer CCD exposures and at a specific time delay from the onset of the LA pulse. This CCD time delay maximizes the DOFMS signal because it allows the signal to be consistently collected when the highest concentration of ablated material enters the ICP-DOFMS instrument from each LA event.

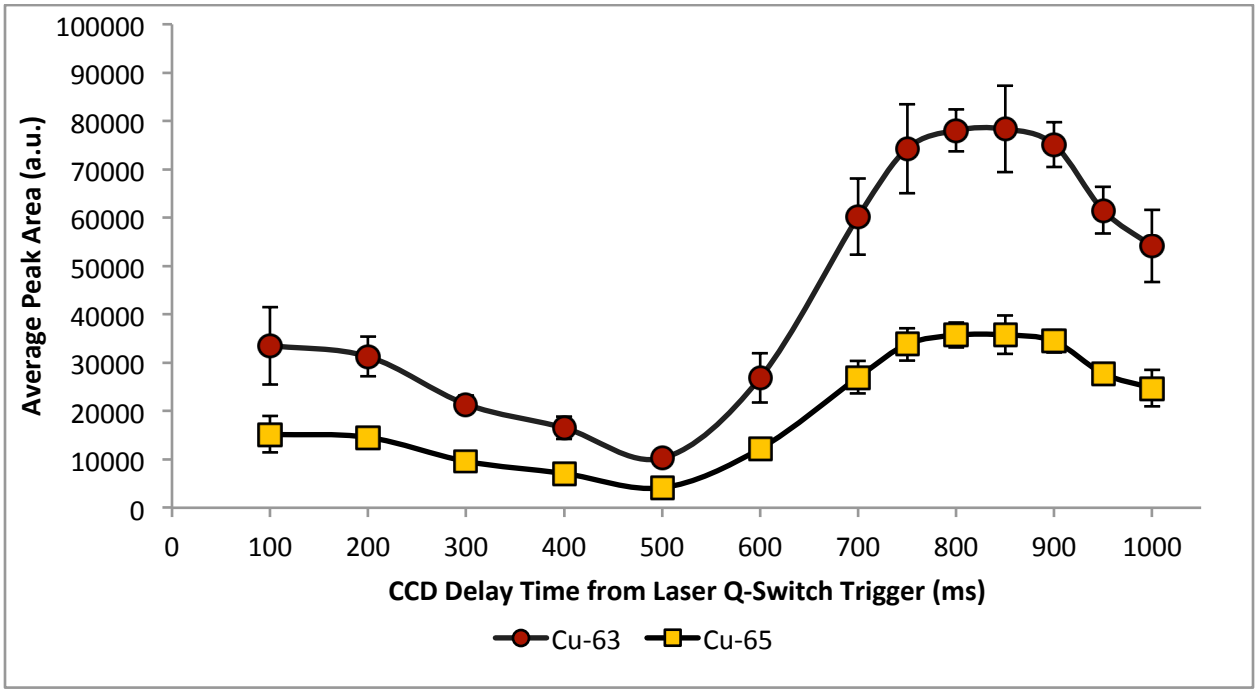

Figure S-2. Average signal vs. CCD delay for analysis of the copper isotopes from the laser ablation of a BNRM Carb20Cb3 standard. Just as with the molybdenum isotopes in Figure 4 of the main text, the maximum signal occurs at a CCD delay time of 800 ms for both ^{63}Cu and ^{65}Cu.

In Figure S-2, integrated signals for the copper isotopes from LA–ICP-DOFMS analysis of the BNRM Carb20Cb3 copper alloy standard are plotted for several CCD delay times. As

shown in the primary report for molybdenum isotopes, the copper isotopic signals peak at a CCD delay of 800 ms. The consistently best CCD-delay time, as well as the very similar delay-dependent signal profile, for Cu and Mo isotopes is a good indicator that the most important factor affecting optimal CCD-delay is the transport time of ablated aerosol from the ablation chamber to the ICP. The helium and argon gas flow rates between the ablation chamber and the ICP torch were the same for the measurements of Mo and Cu; however, the DOF mass analyzer conditions were necessarily different between the two experiments in order to detect each range of masses.

In Figure S-3, a typical DOF mass spectrum obtained with a 100-ms CCD exposure at a single point along the ablation delay-time profile is compared to a spectrum collected with the CCD-delay approach. As seen, the spectrum obtained with the CCD-delay approach has a much better *S/N* ratio, better resolution, and more accurate isotope ratios.

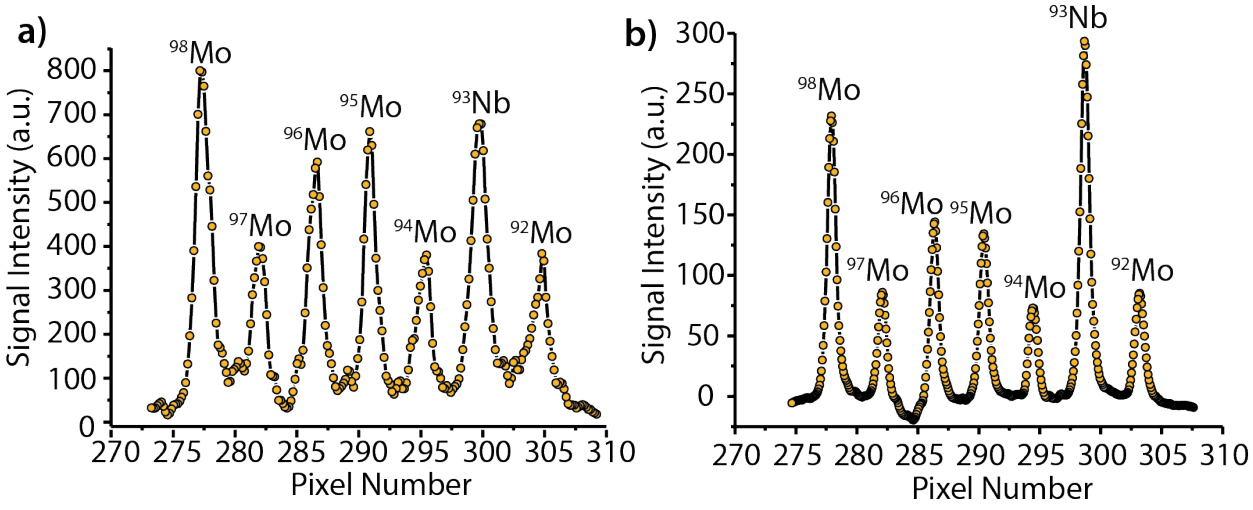

Figure S-3. Comparison of the *S/N* of DOFMS spectra acquired (**a**) with a 100-ms exposure and (**b**) with a 250-ms exposure taken at a CCD delay time of 800-ms from the onset of the laser pulse. The difference in maximum signal between the spectra is due to different gain levels on the MCP/phosphor detector.

Highest Speed LA–ICP-DOFMS

In Figure S-4, we report the highest speed at which LA–ICP-DOFMS spectra were acquired. Here, we fired the laser at 1 Hz; the CCD camera was operated with an exposure of 20-ms and a readout time of 143 ms to produce an overall spectral-collection rate of 6.15 Hz. As seen in Figure S-4, the CCD acquisition rate of 6.15 Hz is fast enough to detect individual laser-ablation events, though not fast enough to consistently detect the signal from the peak of each LA-produced aerosol plug. The large peak-height variation is a result of laser-power variation, ICP drift, and aliasing produced by modulation of the DOFMS signal with the CCD detection readout time. In fact, when the Fourier transform of these data is taken (cf. Figure S-5), the fundamental laser frequency of 1 Hz is apparent at 1 s along with a sideband at 1.14 s due to modulation of the DOFMS signal with the camera readout time of 0.14 s. With the current setup, a maximum speed of ~10 Hz should be achievable; however, these high speeds are possible only for the analysis of high-concentration samples. The 20-ms exposure used to obtain the experiment results in Figure S-4 is possible because copper is the major constituent of the BNRM Carb20Cb3 copper alloy standard. The poor time resolution reported here is not a function of the DOFMS approach, which is capable of delivering 10–20 thousand elemental mass spectra per second. Future incorporation of high-speed, high-sensitivity, and high dynamic-range solid-state DOFMS detectors should improve the temporal response of DOFMS.

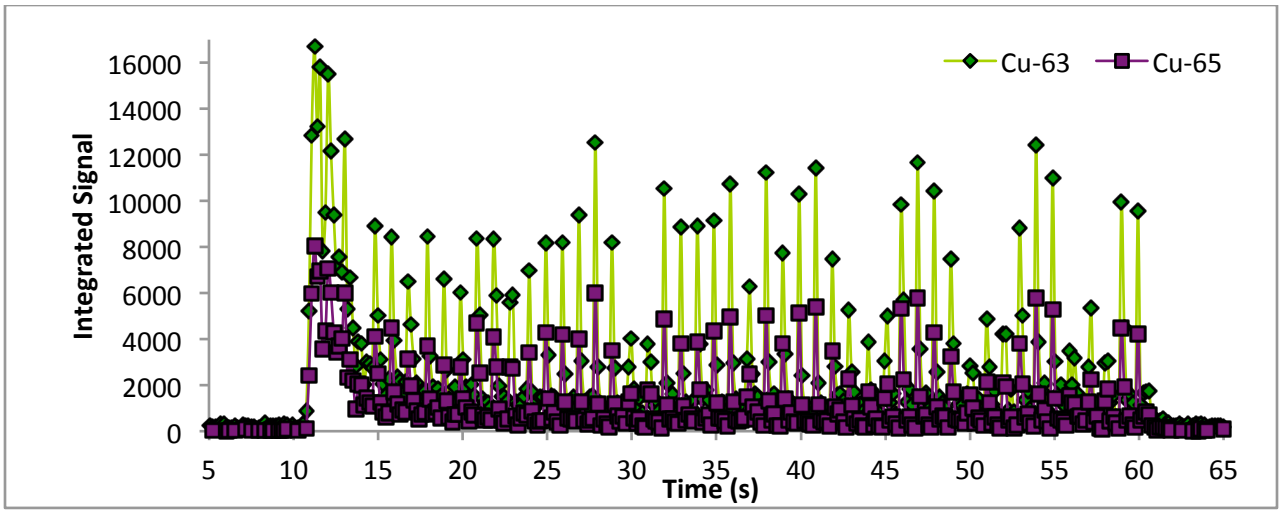

Figure S-4. Fast CCD acquisition at a rate of 6.15 Hz enables the resolution of individual ablation events when the laser is fired at a repetition rate of 1 Hz. A short CCD exposure time of 20 ms is usable here because the sample is composed mostly of copper.

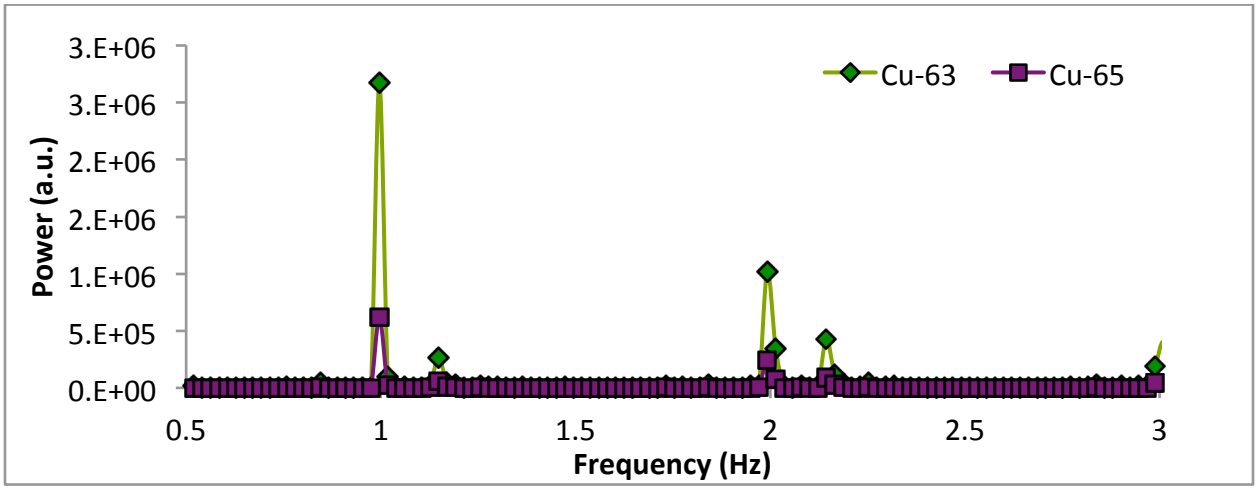

Figure S-5. Fourier transform of data in Figure S-4. Apparent are the fundamental laser pulse frequency of 1 Hz along with a sideband at 1.14 s caused by modulation of the DOFMS signal with the camera readout time of 0.14 s.

References

1. Enke, C. G.; Dobson, G. S., *Anal. Chem.* **2007,** *79* (22), 8650-8661.
2. Graham, A.; Ray, S.; Enke, C.; Barinaga, C.; Koppenaal, D.; Hieftje, G., *J. Am. Soc. Mass Spectrom.* **2011,** *22* (1), 110-117.
3. Graham, A. W. G.; Ray, S. J.; Enke, C. G.; Felton, J. A.; Carado, A. J.; Barinaga, C. J.; Koppenaal, D. W.; Hieftje, G. M., *Anal. Chem.* **2011,** *83* (22), 8552-8559.
4. Enke, C. G.; Ray, S. J.; Graham, A. W.; Dennis, E. A.; Hieftje, G. M.; Carado, A. J.; Barinaga, C. J.; Koppenaal, D. W., *Ann. Rev. Anal. Chem.* **2012,** *5* (1), 487-504.
5. Gundlach-Graham, A. W.; Dennis, E. A.; Ray, S. J.; Enke, C. G.; Carado, A. J.; Barinaga, C. J.; Koppenaal, D. W.; Hieftje, G. M., *Rapid Commun. Mass Spectrom.* **2012,** *26* (21), 2526-2534.
6. Gundlach-Graham, A.; Dennis, E. A.; Ray, S. J.; Enke, C. G.; Barinaga, C. J.; Koppenaal, D. W.; Hieftje, G. M., *J. Anal. At. Spectrom.* **2013,** *28* (9), 1385-1395.
7. Gray, A. L., *J. Anal. At. Spectrom.* **1986,** *1* (3), 247-249.
8. Niu, H.; Houk, R. S., *Spectrochim. Acta B* **1996,** *51* (8), 779-815.
9. Dennis, E. A.; Gundlach-Graham, A. W.; Enke, C. G.; Ray, S. J.; Carado, A. J.; Barinaga, C. J.; Koppenaal, D. W.; Hieftje, G. M., *J. Am. Soc. Mass Spectrom.* **2013,** *24* (5), 690-700.